

$\pi^+$  photoproduction off  $^{16}\text{O}$  and  $^9\text{Be}$  near threshold

E. C. Booth, B. Chasan, F. L. Milder, and B. L. Roberts  
*Department of Physics, Boston University, Boston, Massachusetts 02215*

J. Comuzzi

*Department of Physics and Laboratory for Nuclear Science, Massachusetts Institute of Technology, Cambridge, Massachusetts 02139*  
 (Received 19 June 1979)

The total cross sections relative to photoproduction off the proton have been measured for the reactions  $^{16}\text{O}(\gamma, \pi^+)^{16}\text{N}$  and  $^9\text{Be}(\gamma, \pi^+)^9\text{Li}$  over the energy region from the production threshold up to 12 MeV over threshold. A distorted wave impulse approximation calculation has been performed for the  $^{16}\text{O}(\gamma, \pi^+)^{16}\text{N}$  reaction and is seen to be  $\approx 30\%$  higher than the observed cross section from threshold to 10 MeV. The  $^9\text{Be}(\gamma, \pi^+)^9\text{Li}$  reaction represents the first  $(\gamma, \pi^+)$  measurement near threshold in which the cross section is not dominated by the  $\sigma^2\bar{\epsilon}$  term in the production Hamiltonian.

[NUCLEAR REACTIONS  $^{16}\text{O}(\gamma, \pi^+)^{16}\text{N}$ ,  $^9\text{Be}(\gamma, \pi^+)^9\text{Li}$ , bremsstrahlung end point energies to 175 MeV, measured  $\sigma(E)$ ; calculated  $\sigma(E)$ , DWIA.]

In a recent paper<sup>1</sup> we described a measurement of the total cross section for the reaction  $^{12}\text{C}(\gamma, \pi^+)^{12}\text{B}$  in the threshold region. In this communication we report on the remainder of the threshold total cross section measurements that have been carried out at the MIT-Bates Linear Accelerator. Many of the experimental and calculational details are the same as those in Ref. 1, and these will not be described at length here.

The yield of photopions for  $^{16}\text{O}(\gamma, \pi^+)^{16}\text{N}$  and  $^9\text{Be}(\gamma, \pi^+)^9\text{Li}$  was measured using a bremsstrahlung photon beam. The end point energy of the bremsstrahlung spectrum was varied over the region from below the meson threshold to about 20 MeV over threshold. Targets of  $\text{CH}_2$ ,  $\text{BeO}$ , and beryllium were employed and the resulting photopion yields were analyzed to obtain the total cross sections for  $^{16}\text{O}(\gamma, \pi^+)^{16}\text{N}$  and  $^9\text{Be}(\gamma, \pi^+)^9\text{Li}$ . The  $^{16}\text{O}$  total cross section is compared to a distorted wave impulse approximation calculation using a Helm model description of the nuclear matrix elements taken from inelastic electron scattering.

The experimental arrangement and beam parameters were as described in Ref. 1, except that the photon beam diameter at the pion production target was reduced to 1.9 cm. The methods of data acquisition and data reduction were unchanged. The  $\pi^+$  were not detected directly, but instead, positrons from the decay scheme  $\pi^+ \rightarrow \mu^+ + \nu_\mu$  (mean life  $2.6 \times 10^{-8}$  sec) and  $\mu^+ \rightarrow e^+ + \nu_e + \bar{\nu}_\mu$  (mean life  $2.2 \times 10^{-6}$  sec) were detected after the beam burst.

Since the data were taken with a bremsstrahlung beam, the observed yield was the photon flux above the threshold folded with the total cross section. The yield  $Y(E_0)$  is given by

$$Y(E_0) = \int_{E_T}^{E_0} \sigma(E) \phi(E, E_0) dE, \quad (1)$$

where  $\sigma(E)$  is the total  $\pi^+$  photoproduction cross section,  $\phi$  is the bremsstrahlung flux for an incident electron beam with energy  $E_0$ , and  $E_T$  is the photoproduction threshold. The number of events detected is given by  $(\epsilon\Omega/4\pi)$  times the yield, where  $\epsilon$  is the detection efficiency and  $\Omega$  is the solid angle. Data were taken at 20 end point energies from 150 to 175 MeV. At each end point energy, several measurements of the yield were made for each of the three target materials  $\text{Be}$ ,  $\text{BeO}$ , and  $\text{CH}_2$ .

Two sets of  $\text{CH}_2$  and  $\text{BeO}$  targets were employed. Most of the data were taken using two cylinders approximately 7.5 cm in diameter, one filled with  $\text{BeO}$  powder, the other with  $\text{CH}_2$  pellets. The  $\text{BeO}$  powder had an areal density of 7.91 g/cm<sup>2</sup> and the  $\text{CH}_2$  pellets were 7.66 g/cm<sup>2</sup>. These densities were measured using standard gamma-ray absorption techniques. The second set of targets consisted of solid beryllium,  $\text{CH}_2$  and  $\text{BeO}$ . The solid  $\text{CH}_2$  target was 3.66 g/cm<sup>2</sup> and the  $\text{BeO}$  target was 3.56 g/cm<sup>2</sup>. These thicknesses were measured directly and to check for consistency, the direct measurements were compared to absorption measurements.

It was suspected that water contamination might be present in the  $\text{BeO}$  powder target. To measure the  $\text{H}_2\text{O}$  contamination a solid  $\text{BeO}$  target (containing no water) was employed at energies of 161 and 170 MeV. This target, as well as the solid  $\text{CH}_2$  target, was placed at 45° relative to the photon beam. Whereas the cylindrical diameters of the powdered targets were chosen so that

the attenuation of the exiting positrons were equal for  $\text{CH}_2$  and  $\text{BeO}$ , it was necessary to correct the two sets of data from the solid targets for different positron attenuation. The  $\text{BeO}$  powder was found to contain 0.5%  $\text{H}_2\text{O}$  by weight. We describe our analysis below.

Data were taken at bremsstrahlung end point energies of 161 and 170 MeV using both the solid and powdered  $\text{BeO}$  and  $\text{CH}_2$  targets. This permitted corrections for solid-powder differences as well as a determination of the water contamination in the  $\text{BeO}$  powder. The values for the amount of water contamination at the two different end point energies agreed to within 3%, with statistical errors of 17%. The water contamination per gram per  $\text{cm}^2$  was found to be  $(5.36 \pm 1.56) \times 10^{-3}$ . This small water contamination resulted in as much as a 30% subtraction because of the large  ${}^1\text{H}(\gamma, \pi^+)n$  cross section relative to  ${}^{16}\text{O}$  and  ${}^9\text{Be}$ . However, the internal consistency in the corrections at two different energies gives one full confidence in the subtraction procedure.

In the off line data analysis, several additional corrections were applied to the data: (i) Pion yields and the quantameter values were corrected for photon flux attenuation in the target, (ii) dead time and accidental coincidence corrections were applied, (iii) the solid angle-efficiency factor was

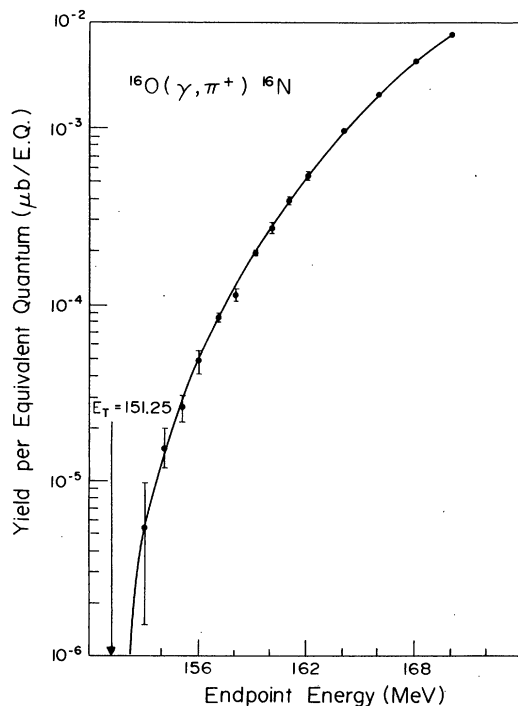


FIG. 1. The  ${}^{16}\text{O}(\gamma, \pi^+){}^{16}\text{N}$  yield per equivalent quantum. The solid curve is the result of a fit as described in the text.

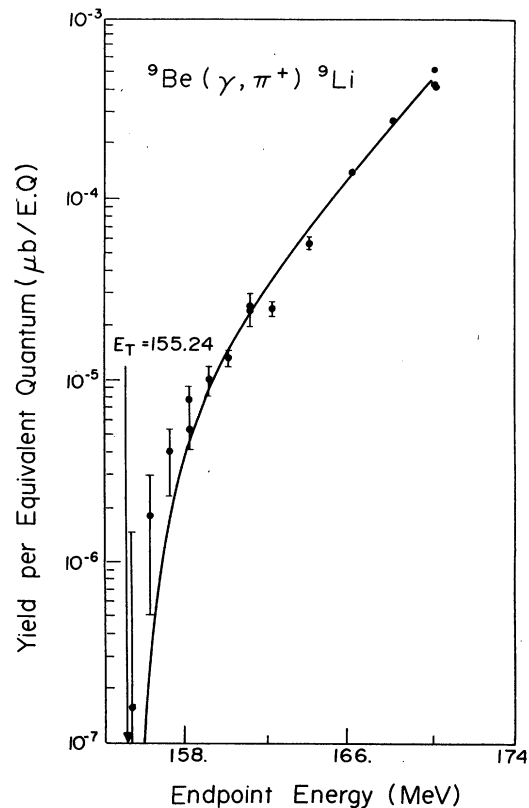


FIG. 2. The  ${}^9\text{Be}(\gamma, \pi^+){}^9\text{Li}$  yield per equivalent quantum. The solid curve is a fit as described in the text.

corrected to include loss of the photopions from the target faces. Muon loss from the targets was neglected as the correction for the two cylindrical targets was of the order of  $10^{-4}$ . The contribution of the carbon to the  $\text{CH}_2$  yield was also neglected, as it was found to be less than a 1% correction.<sup>1</sup>

We define the yield per equivalent quantum per nucleus as

$$\frac{Y(E_0)}{\text{E.Q.}} = \frac{Y(E_0)}{(1/E_0) \int_0^{E_0} \phi(E, E_0) E dE}, \quad (2)$$

where the quantameter charge is proportional to  $\int_0^{E_0} \phi(E, E_0) E dE$ . The yields per equivalent quantum per nucleus for  ${}^9\text{Be}$  and  ${}^{16}\text{O}$  are given in Fig. 1 and Fig. 2. The solid line in each figure is the result of a polynomial fit as explained below.

The  $\text{CH}_2$  data were used to determine the energy calibration as well as the solid angle-efficiency factor. The hydrogen  $(\gamma, \pi^+)$  cross section in the c.m. system near threshold is well known<sup>2</sup> and can be parametrized as

$$\sigma_H = a_H(p/k)(1 - b_H\omega), \quad (3)$$

where  $a_H = 201 \mu\text{b}$ ,  $b_H = 0.0063 \text{ MeV}^{-1}$ ,  $p$  is the pion momentum,  $k$  is the incoming photon momentum,

and  $\omega$  is the photon energy above threshold.  $\sigma_H$  was folded with the bremsstrahlung spectrum,  $\phi$  [see Eq. (1)] to produce a yield as a function of electron lab energy  $E_0$ . A two parameter least squares fit of the calculated yield to the experimental yield provided the solid angle-efficiency factor to  $\pm 5\%$  and the absolute energy scale to  $\pm 50$  keV. Using the solid angle-efficiency factor and the absolute energy scale, the yields for  $^{16}\text{O}$  and  $^9\text{Be}$  were then determined. The  $^{16}\text{O}$  yield was determined by subtracting the normalized Be yield from the BeO yield.

The total cross section was obtained by assuming that the cross section could be parametrized by a polynomial of the form

$$\sigma(E_0 - E_T) = \sum_{j=1}^N C_j (E_0 - E_T)^j, \quad (4)$$

where  $E_0$  and  $E_T$  are energies in the laboratory frame. This polynomial was used to generate yields using Eqs. (1) and (4), and the yield was fitted to the observed yield to determine the best values of the  $C_j$ . Least squares fits were performed for  $N=2, 3, 4, 5$  and the fit with the best normalized chi-square was chosen for the  $^{16}\text{O}$  data. It was necessary to use the 3rd order polynomial fit to the  $^9\text{Be}$  yield since a fluctuation in the Be yield curve at  $E_0 \approx 161$  MeV caused unphysical behavior of the higher order polynomial-generated cross section.

The total cross section obtained from the  $^{16}\text{O}(\gamma, \pi^+)^{16}\text{N}$  yield as discussed above is shown in Fig. 3. Also shown is a distorted-wave impulse approximation (DWIA) calculation that was carried out using a Helm model description for the nuclear matrix elements as discussed in Ref. 1. The Helm model parameters for  $^{16}\text{O}$  were obtained from Graves *et al.*<sup>3</sup> The contribution to the calculated total cross section of each of the  $^{16}\text{N}$  states included in the calculation is shown in Fig. 4. One can see that the dominant contribution in the first few MeV is the  $2^-$  member of the  $^{16}\text{N}$  ground state quartet. This is not surprising as this is a simple spin flip transition from the  $p_{1/2}$  to  $d_{5/2}$  shell and merely shows that close to threshold the production is dominated by the momentum independent  $\vec{\sigma} \cdot \vec{\epsilon}$  term in the production Hamiltonian.

The DWIA calculation for  $^{16}\text{O}$  gives a total cross section that is on the order of 30% higher than the experimental values over the first 10 MeV. This represents considerably greater disagreement with the calculation than was found for  $^{12}\text{C}(\gamma, \pi^+)$ . This may arise from uncertainties in the Helm model parameters for  $^{16}\text{O}$ , or it may be due to a failure of the model itself. Since the  $^{12}\text{C}$  data were quite insensitive to the parameters in the pion-

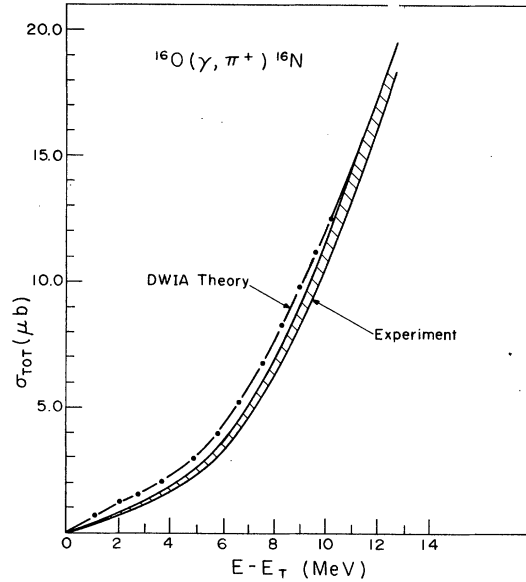


FIG. 3. The measured and calculated total cross sections for  $^{16}\text{O}(\gamma, \pi^+)^{16}\text{N}$ .  $E_T$  is the pion threshold energy and  $E$  is the bremsstrahlung end point energy. The shaded region represents the statistical uncertainty on the cross section. The systematic error is an additional 5%.

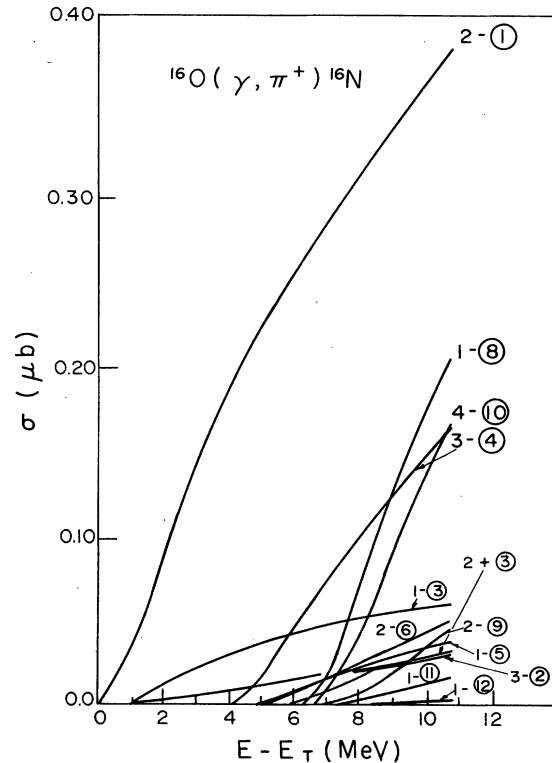


FIG. 4. The contribution of the separate states in  $^{16}\text{N}$  to the total calculated cross section. These were calculated in the DWIA as described in the text.

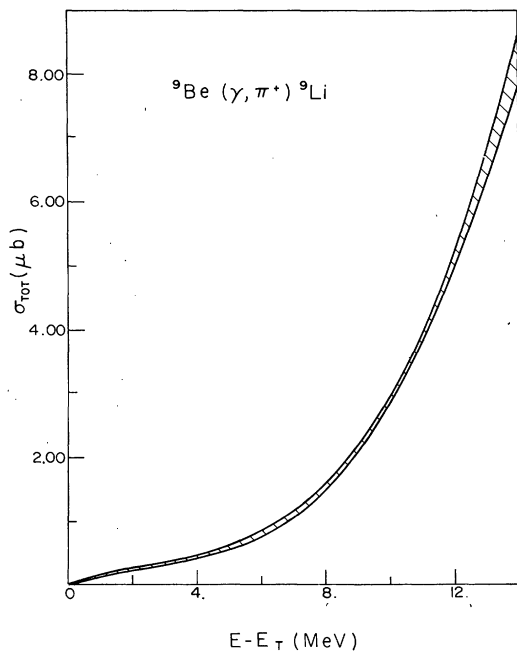


FIG. 5. The measured total cross section for the  ${}^9\text{Be}(\gamma, \pi^+){}^9\text{Li}$  reaction. The shaded region represents the statistical error on the cross section. The systematic error is an additional 7%.

nucleus optical potential, these were not varied in the present calculation for  ${}^{16}\text{O}$ . In both sets of data, one notes a change in slope of the total cross section relative to the calculated one in the energy region 10–12 MeV above threshold. Since this difference appears in both  ${}^{12}\text{C}$  and  ${}^{16}\text{O}$ , it probably signals the onset of quasi-free production or some other channel not included in the calculation.

The  ${}^9\text{Be}$  total cross section is shown in Fig. 5. We note that the  ${}^9\text{Be}(\gamma, \pi^+){}^9\text{Li}$   $\frac{3}{2}^- \rightarrow \frac{3}{2}^-$  transition is not a simple spin flip transition to the ground state of  ${}^9\text{Li}$  and, as such, represents the first  $(\gamma, \pi^+)$  measurement in the threshold region where the cross section is dominated by the momentum dependent terms in the production Hamiltonian. No calculations are available for comparison with these data.

We wish to thank Dr. A. Nagl for a copy of his DWIA code, Mr. G. Franklin for his interest in this experiment and participation in the earlier stages of this work, Dr. P. T. Demos, Dr. W. Turchinets, Mr. Lyman Stinson, and the staff of the Bates Linac for their support throughout the course of these experiments. This work was supported in part by the National Science Foundation and the U.S.D.O.E.

<sup>1</sup>F. L. Milder, E. C. Booth, B. Chasan, A. M. Bernstein, J. Comuzzi, G. Franklin, A. Nagl, and H. Uberall, *Phys. Rev. C* **19**, 1416 (1979).

<sup>2</sup>G. Audit, A. Bloch, N. deBotton, J. L. Faure, C.

Schuhl, G. Tomas, C. Tzara, E. Vincent, J. Deutsch, D. Favart, R. Prieels, and B. van Oystaeyen, *Phys. Rev. C* **16**, 1517 (1977).

<sup>3</sup>R. D. Graves *et al.*, *Can. J. Phys.* (to be published).